Nuclear Engineering and Technology 55 (2023) 1821–1829

Contents lists available at ScienceDirect

Nuclear Engineering and Technology

journal homepage: www.elsevier.com/locate/net

Original Article

Effects of decay heat and cooling condition on the reactor pool natural circulation under RVACS operation in a water 2-D slab model

Min Ho Lee [a], Dong Wook Jerng [b], In Cheol Bang [a, *]

[a] Department of Nuclear Engineering, Ulsan National Institute of Science and Technology (UNIST), 50 UNIST-gil, Ulju-gun, Ulsan, 44919, Republic of Korea
[b] School of Energy Systems Engineering, Chung Ang Univ. Rep. of Korea, 84 Heukseok-ro, Dongjak-gu, Seoul, 06974, Republic of Korea

ARTICLE INFO

Article history:
Received 10 August 2022
Received in revised form
5 December 2022
Accepted 24 January 2023
Available online 24 January 2023

Keywords:
Natural circulation
RVACS
Simulating experiment
2-D slab model

ABSTRACT

The temperature distribution of the reactor pool under natural circulation induced by the RVACS operation was experimentally studied. According to the Bo' based similarity law, which could reproduce the temperature distribution of the working fluid under natural circulation, SINCRO-2D facility was designed based on the PGSFR. It was reduced to 1 : 25 in length scale, having water as a simulant of the sodium, which is the original working fluid. In general, temperature was stratified, however, effect of the natural circulation flow could be observed by the entrainment of the stratified temperature. Relative cooling contribution of the upper plenum (narrow gap) and lower plenum was approximately 0.2 and 0.8, respectively. In the range of decay heat from 0.2% to 1.0%, only the magnitude of the temperature was changed, while the normalized temperature maintained. Boundary temperature distribution change made a global temperature offset of the pool, without a significant local change. Therefore, the decay heat and cooling boundary condition had no significant effect on temperature distribution characteristics of the pool within the given range of the decay heat and boundary temperature distribution.

1. Introduction

Countermeasures for station black out (SBO) accident became more important after Fukushima accident, which was induced by loss of power after tsunami [1]. Therefore, passive decay heat removal systems have been researched based on the natural circulation, which could circulate working fluid and remove decay heat without pumps.

It is common for the liquid metal-cooled reactors (LMRs). There was a system named RVACS, which is an abbreviation of the reactor vessel auxiliary cooling system. It cools decay heat by air natural circulation through the reactor vessel (RV). Decay heat from the core is transferred to the RV by natural circulation of the reactor pool. In other words, the RVACS is a conjugated system of the two natural circulations. It was suggested in the reactor named PRISM, which is a sodium-cooled fast reactor (SFR) [2]. The RVACS could secure two main safety parameters in the LMRs: the maximum coolant temperature and the RV temperature. The maximum coolant temperature is related to adjacent structural integrity and coolant boiling, which could threaten safety shutdown of the reactor. The RV temperature is related to the RV creep failure. By cooling RV by air natural circulation, the RVACS could contribute to secure margins for two main safety parameters.

Regard to in-vessel, it has been researched in terms of natural circulation of the reactor pool itself, with slightly different cooling condition to the RVACS. They were researched with direct heat exchanger (DHX) operation case. In the experimental breeder reactor – II (EBR-II), natural circulation and corresponding decay heat removal were tested under loss of flow and heat sink [3,4]. The PHENIX was a French SFR, and various decay heat removal was tested, and based on the test results, international benchmark was conducted [5,6]. For prototype gen-IV sodium-cooled fast reactor (PGSFR), which is an SFR developing in Korea, STELLA facility was built, and both forced and natural circulation were tested [7].

However, for direct liquid metal, especially sodium, there is a lot of problem in the experiment: large system, high temperature, handling, etc. Therefore, most of the experimental studies for reactor pool natural circulation were conducted as simulating experiments with simulants. The similarity law is based on the reproduction of the temperature distribution under natural circulation, and it was suggested by Grewal et al. [8]. They suggested water as a simulant of sodium for natural circulation with scale reduction, and modified Boussinesq number (Bo') was the key

* Corresponding author.
E-mail address: icbang@unist.ac.kr (I.C. Bang).

https://doi.org/10.1016/j.net.2023.01.021

similarity parameter. It was quantitatively analyzed by Ieda et al. [9], and numerically validated by Eguchi et al. [10], and experimentally validated by Lee et al. [11]. Water could predict liquid metal temperature within approximately 27% of the error. Based on the similarity law, various experimental analysis was conducted. The RAMONA facility was built as 1/20 of the prototype, and temperature distribution of the reactor pool was observed in natural circulation. It was repeated in the NEPTUN facility, which was scaled down to 1/5, and similar results were observed except for reverse flow from the DHX to the core outlet [12,13]. Takeda et al. conducted experiment in 2-D slab model and 3-D model, which were reduced to 1/20. Based on the comparison of the water experiment and numerical results, higher order numerical scheme was suggested for natural circulation [14]. Water model for KALIMER-600 was developed in 1/10 scale with transparent materials to observe velocity field as well as temperature [15]. Particle image velocimetry method was used in PHEASANT, so that both temperature and velocity distribution were observed under natural circulation [16]. For developing lead-cooled fast reactor (LFR) MYRRHA, MYRRHABELLE facility was developed [17].

However, there was few research about natural circulation of the RVACS. Most of LMR natural circulation were researched based on DHX operation condition. Regard to RVACS, most of the research were conducted as numerical study. Nishi et al. analyzed heat removal capacity of the RVACS with CERES code, under SBO [18]. Here, sodium natural circulation was only analyzed in the numerical way, while external air side had an experiment for heat transfer coefficient. Wu et al. analyzed performance of the RVACS regard to Chinese LFR named CLEAR, with RELAP5 code [19]. In the PGSFR, the RVACS design was also analyzed by system code MARS-LMR [20], and CFD [21]. Numerical analysis should be validated against experiments, however, most of the experiments were conducted under DHX condition, not for the RVACS. Therefore, experimental research, especially for RVACS is required for validation of the numerical works, as well as natural circulation itself.

To experimentally analyze natural circulation under RVACS operation, a series of fundamental experiments was conducted. In a 2-D simulating experiments, temperature distribution in the reactor pool under RVACS operation was observed, especially the maximum temperature. Two basic parameters were selected for parametric study: the decay heat level and cooling boundary condition.

2. Experimental method

The natural circulation experiments were conducted in the experimental facility, which was simplified and reduced from the PGSFR, using similarity law. It was named as SINCRO-2D, which is abbreviation of the **SI**mulating **N**atural **C**irculation under **R**VACS **O**peration – **2D**. In this section, the similarity law and design of the SINCRO-2D was discussed, and test matrix was determined based on the actual RVACS operation condition.

2.1. Similarity law and simulant

Key for the similarity is the modified Boussinesq number (Bo'), which is the ratio of the heat transferred by the natural convection to conduction. By matching Bo', the temperature distribution under natural circulation could be simulated. Its derivation and validation experiments were discussed in detail by Lee et al. [11]. Equations (1)–(3) showed non-dimensionalized form of the three governing equations: mass, momentum and energy, respectively. Here, two non-dimensional numbers were derived; the modified Grashof number (*Gr*') and Bo', which were defined in equations (4) and (5).

$$\frac{\partial u_i^*}{\partial x_i^*} = 0 \tag{1}$$

$$\frac{\partial u_i^*}{\partial t^*} + u_j^* \frac{\partial u_i^*}{\partial x_j^*} = \frac{1}{Gr'^{1/2}} \frac{\partial^2 u_i^*}{\partial x_j^{2*}} - \frac{\beta g \Delta T_{ref} L}{u_{ref}^2} T^* \delta_{i3} - \frac{\Delta P}{\rho u_0^2} \frac{\partial P^*}{\partial x_i^*} \tag{2}$$

$$\frac{\partial T^*}{\partial t^*} + u_j^* \frac{\partial T^*}{\partial x_j^*} = \frac{1}{Bo'^{1/2}} \frac{\partial^2 T^*}{\partial x_j^{2*}} + \frac{Q_0 L}{\rho c_p u_{ref} \Delta T_{ref}} - \frac{Q''}{\rho c_p u_{ref} \Delta T_{ref}} \tag{3}$$

The *Gr*' is related to the flow regime, similar to the Reynolds number. The Bo' was in the diffusion term of the non-dimensionalized energy equation, thus, it is related to the temperature distribution. Here, the fact that temperature distribution could be reproduced without matching *Gr*' was already suggested by Ieda et al. [9], and experimentally proven by Lee et al. [11]. And most of the facilities were designed based on Bo' [9–14,16]. Therefore, the Bo' was the most important number for the temperature similarity, and further discussion about similarity and design of the facility were based on only Bo'.

$$Gr' = \left(\frac{\beta g}{\rho c_p}\right)^{2/3} \frac{L^{4/3} Q^{2/3}}{\nu^2} \tag{4}$$

$$Bo' = \left(\frac{\beta g}{\rho c_p}\right)^{2/3} \frac{L^{4/3} Q^{2/3}}{\alpha^2} \tag{5}$$

As shown in the definition of the Bo', in equation (5), it could be expressed as material properties and system properties. Making volumetric heat generation rate as constant, the relative length scale for identical Bo' could be determined by only depending on the material properties. Length scales with various working fluids were summarized in Fig. 1. The scale was defined as relative length scale to have the same Bo' with water, therefore, water was set as 1. If the relative length scale is smaller than 1, the size of the system should be smaller than that of the water and vice versa. Compared to water, metals have much higher thermal diffusivity, which is in the denominator in equation (5). Other properties have less significant difference than thermal diffusivity. Therefore, the size of the metal system should be larger than the water system because the size is in the denominator. There are five kinds of working fluids; heat transfer oil, liquid metal, heat transfer salt, refrigerant, and water. For heat transfer oils, which is golden colors in Fig. 1, to match Bo', the scale should be less than 1/50. Excessive scale reduction has disadvantages in terms of handling of the experiment, geometrical similarity, and transparency. For refrigerants,

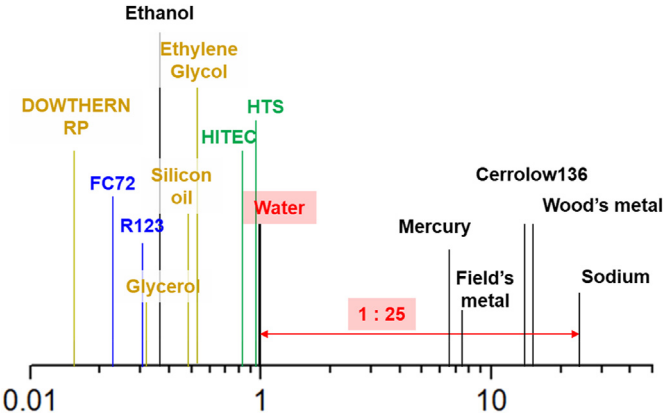

Fig. 1. Relative length scale for identical Bo' [11].

which were blue in Fig. 1, they are relatively free from transparency and visualization, however, their boiling point is too low for operation under the atm. Molten salts (green) are also opaque and hard to be maintained as a liquid state due to its high melting point. Liquid metals, which are in the right side of the figure have similar properties with original coolant, sodium, except for density. Different to the aforementioned three fluids, it requires smaller scale difference with sodium, which makes disadvantages in terms of the scale reduction of the system. Toxicity, cost and handling problem are other difficulties in the liquid metals. Ethanol has no advantages compared to the water. Therefore, water is the best working fluid for scale-down experiments in the aspect of visualization and length scale. As many literatures did, water was selected as a simulant of the sodium, having 1 to 25 of the scaling ratio.

2.2. Experimental facility

For pool type SFRs, natural circulation flow under RVACS operation was formed through the IHX region. Under accident, the IHXs are isolated and there is no heat removal through the IHXs, which means that the IHXs are just flow path for the natural circulation. Sodium coolant is heated up in the core and flow into the upper plenum. The sodium was cooled by the RV wall in both hot pool and cold pool, while flowing from the upper plenum to the lower plenum through the IHX. It finally re-enters to the core through the pump and inlet plenum. This natural circulation flow path was considered during the design of the experimental facility, SINCRO-2D. Fig. 2 shows the schematic of the SINCRO-2D and PGSFR. Named in grey color components: pump, DHX, and perforated plate, were not reflected into the SINCRO-2D, because they have little effect on the natural circulation flow. The DHX was intentionally excluded to concentrate on the natural circulation with the RVACS. The IHX and inlet plenum were simulated as simplified pipe with proper diameter for identical pressure drop coefficient.

Based on the PGSFR, SINCRO-2D has been developed in 1/25 scale of the prototype in an isotropic manner. Table 1 shows comparison of the specification of PGSFR and SINCRO-2D. Power density was maintained in the facility. In this power and length ratio,

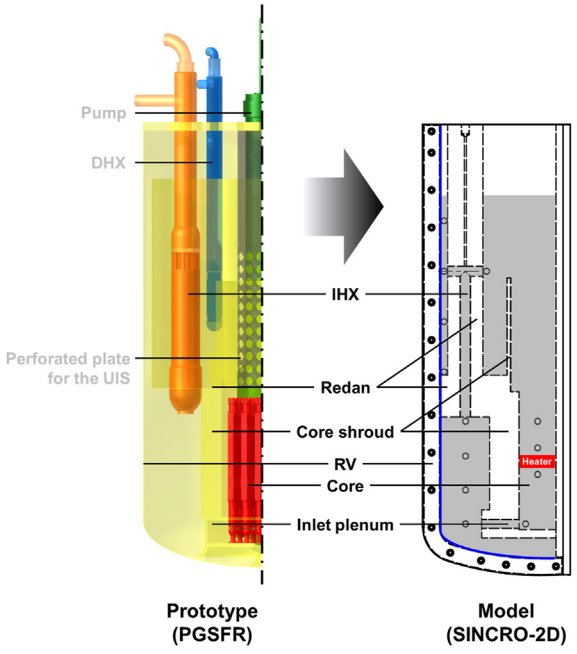

Fig. 2. Schematic of the SINCRO-2D.

the most important similarity parameter Bo', showed good accordance as 1 : 1.25. The reference temperature difference was derived during non-dimensionalization like equation (6). Corresponding scaling ratio of the temperature difference was 0.162, which means that 1 °C of the temperature difference in the SINCRO-2D is equivalent to 6.16 °C in the prototype.

$$\Delta T_{ref} = \left(\beta g \rho^2 c_p^2 L^5\right)^{-1/3} Q^{2/3} \tag{6}$$

2.3. Test matrix

RVACS uses natural circulation so that it requires some time for its operation [10]. Considering setup time of the RVACS, decay heat level was determined from 1% of the total power, which is decay heat level at the 8.8 h after shutdown [11]. Experimental conditions were from 1% of the decay heat to 0.2% of the decay heat and corresponding power at the SINCRO-2D and time after shutdown are summarized in Table 2. All the cases were under steady state.

Cooling boundary condition is also crucial for the sodium pool natural circulation of the RVACS. In the aspect of the temperature difference between RV and sodium, temperature distribution is more dominant than average temperature. In the SINCRO-2D, a 2-D slab model, only axial temperature distribution could be considered. Here, upper part of the cooling wall had always higher temperature than the lower part considering flow direction of the pool and cooling jacket. Therefore, the temperature distribution was simplified as a temperature difference between the top and bottom of the cooling wall. Temperature difference between the top and bottom could be represented as reference temperature difference in equation (6). There have been few researches about temperature distribution of the RV so that it was assumed by range of the possible temperature difference. In terms of the heat transfer, the RV is related to the reactor pool and air channel. Therefore, possible range of the temperature difference was assumed as the temperature difference along the pool or the air channel. Kraus et el. Reported 65 °C of pool temperature difference under natural circulation of the PGSFR [22]. From the simple calculation, with 1% of the decay heat, the pool temperature difference showed 77 °C–155 °C, as flow rate changes 0.5%–1% of the normal operation. Approximately 140 °C of the temperature difference was observed between inlet and outlet of the air channel [20]. Therefore, possible range of the maximum temperature difference between the top and the bottom of the RV would be 65 °C–155 °C, which corresponds to $42.5\Delta T_{ref}$ to $101.4\Delta T_{ref}$ in equation (6). Based on this result, test matrix regard to the boundary condition was determined like Table 3, from 40 to 100 times of the ΔT_{ref}, with $20\Delta T_{ref}$ of the interval.

2.4. Uncertainty analysis

Uncertainty analysis was based on the general error propagation method. Three parameters were controlled or observed in this study: the power, flow rate, and temperature. Each contributor and

Table 1
Specification of the SINCRO-2D.

Parameter	PGSFR	SINCRO-2D	Ratio
Radius	4.3 m	173 mm	1/25
Height	15.3 m	540 mm	1/25
Power density	213.4 W/cm^3	213.4 W/cm^3	1
Bo'	0.86×10^8	1.07×10^8	1/1.25
ΔT_{ref}	1.528 °C	0.248 °C	0.162

Table 2
Test matrix – Decay heat.

Time after shutdown	Decay heat to the total power	SINCRO-2D power
8.8 h	1.0%	200 W
17.1 h	0.8%	160 W
33.2 h	0.6%	120 W
64.4 h	0.4%	80 W
124.9 h	0.2%	40 W

Table 3
Test matrix – Boundary condition.

Normalized ΔT_{ref}	$\Delta T_{top,bottom}$ in PGSFR	$\Delta T_{top,bottom}$ in SINCRO-2D
40	61.12 °C	9.92 °C
60	91.68 °C	14.88 °C
80	122.24 °C	19.84 °C
100	152.80 °C	24.79 °C

total uncertainty for these parameters were summarized in Table 4. The heating was governed by a DC power supplier as voltage control, with a constant resistance of the heater. Both voltage and resistance were measured by a multimeter from Agilent, U1241B. According to the resolution of the multimeter, voltage uncertainty was 0.09% of the reading, while resistance uncertainty was 0.20% of the reading. Therefore, the total uncertainty in the power was approximately 0.27%. To measure coolant flow in the water-cooling channel, KTM-100 from the Kometer was used. It has 1.00% of the full-scale error, which corresponds to 0.15 L per minute (lpm). 250 Ω resistance was employed to convert 4–20 mA to measurable voltage, having 1.00% of the uncertainty. The Agilent 34980A and 34,921 were used as data acquisition system (DAS), which has 0.004% of the DC voltage accuracy and 22-bit analogue to digital conversion. With 10 V of the measurement range, the uncertainty at the interface was 0.01%. 22 bits of analogue to digital converting resulted 0.00% of the error. Considering 2.8 to 9.2 lpm of the flow range in the experiment, total uncertainty in the flow rate was varied from 1.91 to 5.44% because uncertainty from the flowmeter was proportional to the full scale, while the other contributors were based on reading. The uncertainty of the K-type thermocouple was 0.4% of the reading. A contribution from the class 1 compensation wire was 1.5K, and another contribution from the reference temperature were 1.0 K, which was specified by the DAS. The other contributors were 0.01% from the interface and 0.01% from the analogue to digital conversion. Considering all these factors, final uncertainty in the temperature was 2.01–2.07 K, within the experimental temperature range from 20 °C to 50 °C.

In addition to the basic uncertainties, temperature fluctuation during experiment is summarized in Fig. 3. The magnitude of fluctuation is determined by the natural circulation flow and corresponding temperature distribution. For example, if a hotter fluid is supplied from the bottom, the temperature will be significantly fluctuated. At the core outlet, the hottest fluid from the heater flew into the upper plenum, which induced large disturbance of the temperature. Thus, temperature fluctuated approximately 1.5 °C. It was larger in the IHX T junction, as approximately 2.5 °C, because the cold and hot fluid mixed, For the IHX outlet, relatively hot fluid came down to the lower plenum, and had 1 °C of temperature fluctuation. There was weak flow in the lower plenum and small temperature gradient in the inlet piping. Therefore, these two points had small fluctuation. The core inlet also had small fluctuation due to its favorable temperature stratification although there was significant upward flow. Natural circulation flow itself would be discussed in section 3.2 in more detail.

Table 4
Summary of uncertainty contributors.

Category	Contributor	Magnitude
Power	Voltage	0.09% of reading
	Resistance	0.20% of reading
	Total	0.27%
Flow rate	Transmitter	1.00% of full scale
	Resistance	0.10% of reading
	I/O interface	0.01% of full scale
	AD conversion	0.00% of full scale
	Total	1.91–5.44%
Temperature	Thermocouple	0.40% of reading
	Compensation wire	1.5 K
	Reference temperature	1.0 K
	I/O interface	0.01% of full scale
	AD conversion	0.00% of full scale
	Total	2.01–2.07 K

3. Results and discussion

3.1. Estimation of the boundary temperature

Before discussion on the results, the boundary condition should be estimated. For the natural circulation inside of the SINCRO-IT, the boundary condition is temperature distribution of the cooling boundary, which corresponds to the T_{wall_in} Fig. 4. As discussed in test matrix, it was simplified as temperature difference between the top and bottom of the cooling surface. The top of the cooling boundary corresponds to the top of the pool and outlet of the water cooling jacket, while the bottom corresponds to the bottom of the pool and inlet of the cooling jacket. However, it could not be directly measured, thus, it was evaluated by using a thermal circuit like equation (7).

$$\Delta T_{boundary} = T_{RV,top} - T_{RV,bottom} \tag{7}$$

$$T_{RV,bottom} = T_{coolant,in} + \Delta T_{coolant-wall,bottom} + \Delta T_{wall,bottom} \tag{8}$$

$$T_{RV,top} = T_{coolant,out} + \Delta T_{cooling,top} + \Delta T_{wall,top} \tag{9}$$

The temperature of the bottom and top of the RV could be expressed like equations (8) and (9), respectively. Here, inlet temperature and adjacent SINCRO-2D pool temperature was almost the same. Since temperature difference between the pool and coolant was nearly zero, heat flux through the wall could be treated as zero. However, for the top, the two ΔT could not be neglected. They could be expressed like equations (10) and (11), respectively. Final form of the temperature difference along the cooling boundary could be expressed like equation (12).

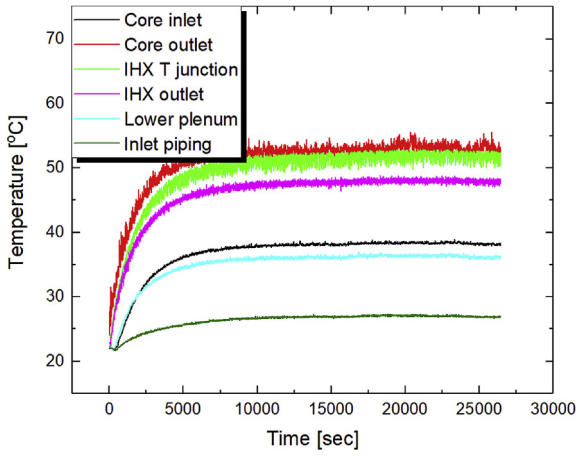

Fig. 3. Temperature history of the base case (1.0%, 60ΔT_{ref}).

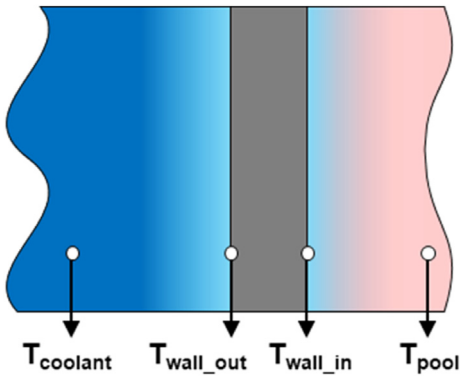

Fig. 4. Schematic of the temperature point near the cooling boundary.

$$\Delta T_{coolant-wall,top} = \frac{q''}{h_{coolant-wall,top}} \tag{10}$$

$$\Delta T_{wall} = \frac{q'' d_{wall}}{k_{wall}} \tag{11}$$

$$\Delta T_{boundary} = \Delta T_{coolant\ in-out} + q'' \left(\frac{1}{h_{coolant-wall,top}} + \frac{d_{wall}}{k_{wall}} \right) \tag{12}$$

However, heat transfer coefficient (HTC) between the wall and coolant should be validated against the experimental data. The data were from the base case, 1.0% of the decay heat with $60\Delta T_{ref}$ of the boundary condition. Because the thermocouples were installed in the coolant channel and the pool, temperature of the wall should be calculated using correlation and the validity of the correlations should be checked. The validation of the HTC should include measurable two points. Considering thermal circuit including these two points, it would be like equation (13), which contains another HTC between the pool and wall.

$$T_{pool} = T_{coolant,out} + q'' \left(\frac{1}{h_{coolant-wall,top}} + \frac{d_{wall}}{k_{wall}} + \frac{1}{h_{wall-pool,top}} \right) \tag{13}$$

$$h_{coolant-wall} = \left(\frac{k}{L_c} \right) \frac{(f/8)(Re_D - 1000)Pr}{1 + 12.7(f/8)^{1/2}\left(Pr^{2/3} - 1\right)} \tag{14}$$

$$h_{wall-pool} = \left(\frac{k}{L_c} \right) \left[0.825 + \frac{0.387 Ra^{1/6}}{\left\{ 1 + (0.492/Pr)^{9/16} \right\}^{8/27}} \right]^2 \tag{15}$$

$$f = (0.79\ ln(Re_D) - 1.64)^{-2} \tag{16}$$

For HTC between the coolant wall, Gnielinski correlation was used because it includes the lowest Re among the correlations. Actually, Re_D in the cooling jacket was approximately 2300. It was slightly lower than fully turbulent flow, however it was surely turbulent because there were contributors for the turbulent: curved channel and perpendicular channel inlet. Therefore, the correlation was determined as having the lowest Re range, which was the Gnielinski correlation. Regard to HTC between the wall and the pool, general Churchill and Chu correlation was employed. The correlations and the related parameter were summarized in equation 14–16.

For the HTC between the coolant wall, fin effect should be considered because the adjacent walls of the channel could act like fins. The schematic of the fin effect of the wall is in Fig. 5. Thickness of the fin was 5 mm per each while its length was 21 mm. Original HTC was calculated as 258.8 W/m^2. K, while considering fin effect, it was increased 1.55 times, 494.3 W/m^2.K. The HTC between the wall and pool was evaluated as 665.1 W/m^2.K.

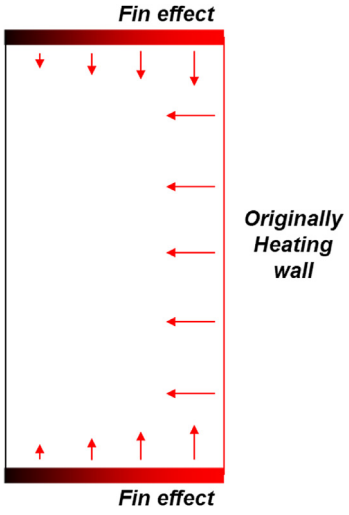

Fig. 5. Schematic of the fin effect.

Heat flux in equation (13) could be obtained using experimental data. Approximately 20% of the heat (40 W) was removed in the narrow gap of the upper plenum, whose area was 56.25 cm^2. Therefore, heat flux could be assumed as approximately 7 kW/m^2.

Finally, it was calculated as 25.1 °C of the temperature difference between the coolant and the pool, using correlations, while 25.5 °C was observed in the experiment. Therefore, it could be concluded that correlations for the HTCs were adequately selected. Further discussions on the boundary temperature of the SINCRO-2D were based on the calculation of the HTC between the coolant and wall.

3.2. Heat balance and base case analysis

Heat balance of the facility after insulation was tested with 1.0% of the decay heat with $60\Delta T_{ref}$ of the boundary condition, which was called as the base case. Insulation rate of the facility could be calculated using equation (17). To minimize random error, mass flow rate and temperature difference was obtained as average of 25 moments of the steady state. During steady state, the data were obtained five times, and the results of the insulation test were summarized in Table 5. The average insulation rate of the SINCRO-IT was 97.4% so that further analysis were based on the ideal insulation.

$$Insulation\ \ rate = \frac{Q_{cooling}}{Q_{input}} = \frac{\dot{m} c_p \Delta T_{coolant,in-out}}{Q_{input}} \tag{17}$$

Fig. 6 shows the temperature distribution of the pool of the base case. Temperature distribution was stratified in general. Using this thermal stratification, the natural circulation flow could be estimated. If there is no flow, the temperature would be fully stratified. However, there were several regions where stratified temperature was entrained by the natural circulation flow. The natural circulation formed in the order of the core outlet – upper plenum – IHX (narrow gap) – lower plenum – inlet piping – core inlet. From the core outlet, temperature was maintained near 53 °C in the upper plenum, and to the inlet of the IHX. The maximum temperature was 53.3 °C. There was a narrow gap between the IHX and the cooling wall. Temperature stratification was also observed in the narrow

gap, however, the magnitude of the temperature was quite different to the other region because it was connected to the other part of the pool through the small IHX. In the IHX, there was mixing of the water from the upper plenum and narrow gap at the T-junction of the IHX. After the mixing, the water cooled down to 47.6 °C, which was observed at the outlet of the IHX. In the lower plenum, the temperature was stratified, with sudden gradient between the last two points. It could be assumed as an effect of the natural circulation. Downward flow from the IHX outlet entrained the stratified temperature, so that there was sudden temperature change where the effect of the downward flow was sufficiently attenuated. The minimum temperature in the natural circulation flow was observed after the inlet piping, which was 26.9 °C. Then, the cooled water went upward to the heater. The points 36.1 °C and 26.9 °C were located at the same height, however, temperature was quite different. It was another evidence of the effect of natural circulation on the stratified temperature profile. The effect of the flow on the temperature distribution could represented by entrainment of the temperature by the counterclockwise circulating flow.

There were two regions which did not participated of the natural circulation. First, it was obvious that the bottom of the pool did not participate considering its shape, location and 17.2 °C of the temperature. The other regions were the bottom of the narrow gap. The temperature was also stratified in the narrow gap. However, natural circulation occurred at only upper two points. If there was downward flow from the second to the third points, it should have lower temperature than 35.2 °C due to additional cooling. And this colder fluid could not move upward itself because there was hotter fluid above the colder fluid. Therefore, the water was stagnated and continuously cooled in the narrow gap below T-junction, and only upper part of the narrow gap participated into the natural circulation.

Before the experiment, it was presumed that conduction is dominant heat transfer mechanism in the hot pool cooling because the distance between the narrow gap and the T-junction of the IHX was relatively smaller than others. To evaluate heat transfer mechanism in the narrow gap, simple 1-D calculation was conducted. Heat transferred amount by the conduction was evaluated and it would be compared to the total power, temperature decrement after the IHX, and calculated heat removal fraction at the narrow gap, which would be calculated later. The thermocouple at the T-junction of the IHX and at the narrow gap having same height with the T-junction of the IHX were selected to calculate the amount of conduction, which have temperature as 52.0 °C and 35.2 °C, respectively. The distance between these two points was 30 mm. Thermal conductivity of the water was 0.6 W/m.K. The area of the IHX channel was 176.7 mm^2. From these parameters, only 0.06 W of the heat was transferred by solely conduction in this distance. However, temperature dropped from 52.8 °C at the IHX inlet to the 47.6 °C at the IHX outlet. The amount of the conduction was 0.06 W, and it was too small to make such a significant cooling. Therefore, there should be another cooling mechanism, the natural circulation. The natural circulation was dominant even in the narrow gap, and natural circulation was the dominant heat mechanism

Table 5
Summary of the insulation test of the SINCRO-2D.

Test	Insulation rate
1	96.9%
2	96.6%
3	98.7%
4	101.9%
5	93.1%
Average	**97.4%**

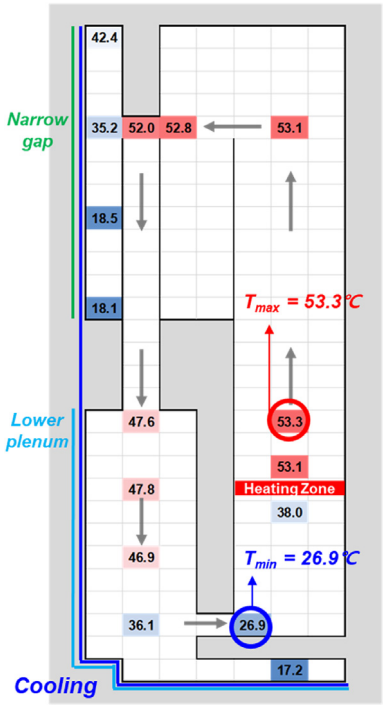

Fig. 6. Temperature distribution of the base case (1.0%, 60ΔT_{ref}).

for the overall pool.

The contribution to the cooling of the narrow gap and IHX could be calculated using temperature change during the natural circulation. The maximum temperature was 53.3 °C at the core outlet, while the minimum temperature was 26.9 °C at the inlet piping. It means that total 26.4 °C of the temperature increased through the core, and decreased through the other parts of the natural circulation flow path. Here, the temperature at the outlet of the IHX was 47.6 °C. It means that the hot flow from the core was cooled down by the cooling at the narrow gap, from 53.3 °C to 47.6 °C. In other words, 5.7 °C of the temperature was decreased by the narrow gap cooling. In the viewpoint of the lower plenum, 47.6 °C of the coolant was entered to the lower plenum and went out to the inlet piping with the temperature of the 26.9 °C. It means that 20.7 °C of the temperature was cooled down in the lower plenum. From the temperature change history along the natural circulation path, cooling fraction could be calculated using equation (18).

$$Cooling\ fraction = \frac{(T_{inlet} - T_{outlet})_{component}}{(T_{max} - T_{min})_{system}} \tag{18}$$

As a result, 20.8% of the heat was removed at the narrow gap, and it corresponds to 41.6 W of the heat was cooled at the narrow gap. The other 79.2% of the heat, which is 158.4 W, was cooled at the lower plenum. The cooling fraction can suggest importance of the internal structure in the natural circulation. In general, higher part of the pool has the higher temperature than the lower part of the pool. If there was no internal structure disturbing natural circulation flow in the pool, cooling heat flux is higher in the higher region because the heat flux is proportional to the temperature difference between the pool and the boundary. However, in the SINCRO-2D experiment, most of the heat was removed in the lower part of the pool, the lower plenum. The small cooling fraction of the narrow gap was caused by the internal structures which disturb the flow to the upper cooling wall.

For the direct data interpretation between the results of the

SINCRO-2D and the PGSFR, some points should be considered. The geometrical similarity was distorted by two-dimensionalization. There are four IHXs in the PGSFR, however, only one IHX was reflected into the SINCRO-2D design. Inlet piping including pump was much more complex than simplified one. It means that the pressure drop related of the IHX were not strictly simulated. In addition, ratio of the core to the cooling surface was distorted. To have exact symmetry with the original three-dimensional reactor, the experimental facility should be a circular segment, like a piece of a pizza. However, SINCRO-2D was 2-D slab model. Therefore, the volume of the core was overestimated, while the area of the cooling surface was underestimated. Therefore, the results of the SINCRO-2D experiment could not be directly interpreted to those of the PGSFR. However, since the SINCRO-2D had the same Bo' with prototype, the present experiment could give enough physical insights for the natural circulation phenomena under the RVACS operation condition, especially for the dominant cooling mechanism in the narrow gap and the cooling contribution of the lower plenum.

3.3. Effect of decay heat

Considering 0.65% of the maximum heat removal capacity of the PGSFR, an effect of decay heat was parametrically studied from 0.2% to 1.0%, with 0.2% of the interval. Cooling boundary condition was fixed as $60\Delta T_{ref}$. The results were summarized in Fig. 7. Overall temperature distribution tendency was not significantly changed, and only magnitude of the temperature distribution was changed.

$$\theta = \frac{T - T_{boundary}}{\Delta T_{ref}} \tag{19}$$

For more quantified analysis and detailed analysis, temperature was normalized to the reference temperature (equation (6)) at each power level. It is the temperature difference between the boundary and a point over the reference temperature. Normalized temperature difference (θ) was summarized in Fig. 8, and there was no significant difference with different power level. In case of the relatively high power like 0.6, 0.8, and 1.0%, the θ were very similar through all regions. For small power like 0.2 and 0.4%, they showed more uneven θ distribution than that of the higher power. High temperature region like the core outlet and IHX T-junction showed higher θ, and lower temperature region like the core inlet and lower plenum showed lower θ. This uneven θ was more significant in the lower temperature region in terms of the ratio. Regard to the maximum temperature, which was observed at the core outlet, compared to the base case with 1.0% of the power, the θ at 0.2% showed higher than approximately 20, which is 15% smaller. However, in case of the core outlet, θ differences between 0.2% and 1.0% was approximately 24, which is 33% smaller than 1.0%. For the lower plenum, θ difference was 26, which is 40% smaller. Discordance of the θ was caused by the water property change along the temperature, especially, the viscosity. The average temperature between the core inlet and outlet of the 1.0% case was 45.6 °C and the viscosity of the water is 0.59 mPa s. In case of 0.2%, the average temperature was 28.9 °C, where water viscosity is 0.82 mPa s. Due to pressure relative drop increase in the lower power by larger viscosity made temperature distribution of the natural circulating pool more uneven, and it was more significant in the lower temperature regions.

3.4. Effect of boundary condition

The cooling boundary condition effect was observed with a fixed power of 1.0%. Temperature distribution with various boundary conditions were summarized in Fig. 9. Since the power was fixed as 1.0%, magnitude of the temperature was quite similar in all cases. Moreover, tendency of the temperature distribution did not change, and the graph was only shifted upward and downward while the boundary condition changed. It could be concluded that cooling fraction and heat transfer characteristics were also not changed. Therefore, the effect of the boundary temperature distribution could be simplified as a global offset of the temperature inside of the pool.

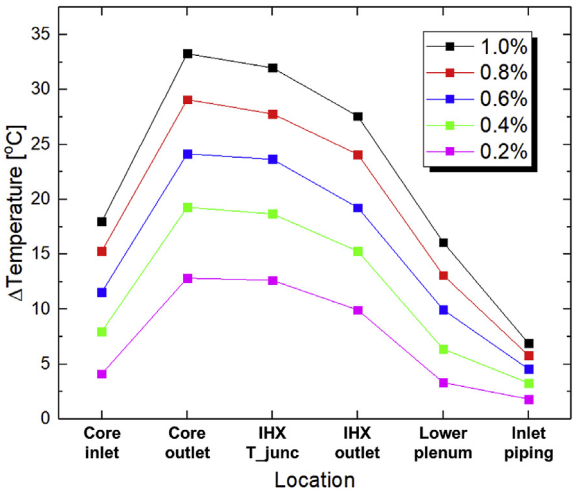

Fig. 7. Temperature distribution in the pool with various decay heat.

To quantify the global temperature offset by boundary condition, temperature of an arbitrary point of the pool could be expressed like equation (20). Here, to apply the effect of the boundary condition as a global offset, a representative RV temperature, which is $T_{RV,representative}$ in equation (20), should be maintained without change as the boundary condition changes. In the results of the parametric study on the boundary condition effect, the global temperature offset could be observed solely because the power was fixed as 1.0%. So that temperature increase by decay heat was constant during the parametric study. Thus, if the representative RV temperature and temperature offset by the boundary condition were subtracted from the pool temperature, it should be constant. For clear comparison, the pool temperature was fixed as the maximum pool temperature, and equation (20) was rearranged as (21).

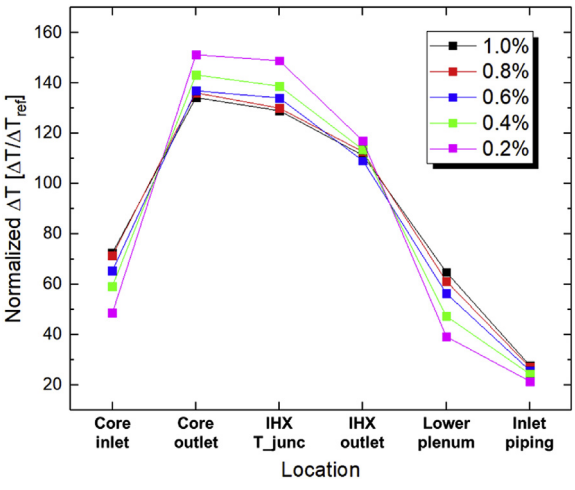

Fig. 8. Normalized temperature distribution in the pool with various decay heat.

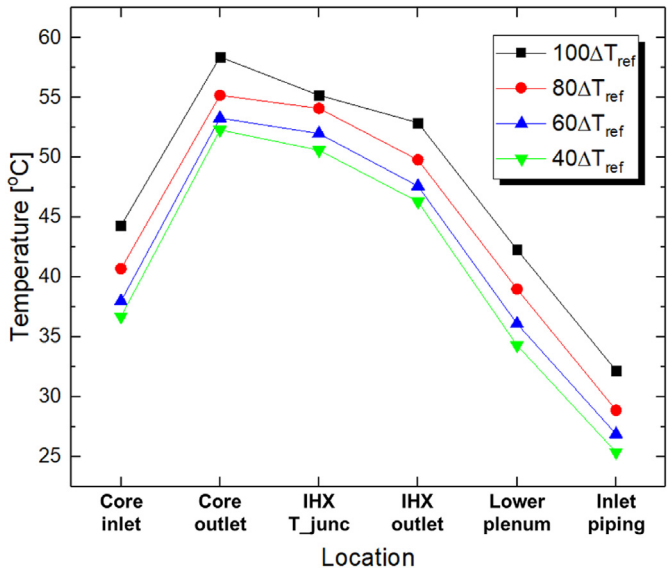

Fig. 9. Temperature distribution of the pool with various cooling boundary condition.

$$T_{pool} = T_{RV,representative} + \Delta T_{by\ power} + \Delta T_{by\ boundary} \quad (20)$$

$$T_{pool,max} - T_{RV,representative} - \Delta T_{by\ boundary} = \Delta T_{by\ power} \quad (21)$$

Various candidates for the subtraction terms on the left-hand side of equation (21) were considered and summarized in Table 6. The table contains the value of the left-hand side of equation (21), therefore, it should be constant even boundary condition was changed. First, the temperature at the top of the RV, which was the maximum, was considered. However, the result in the table showed change of the calculation results with different boundary conditions. It means that the effect of the boundary condition was not properly reflected, and the representative RV temperature was not assumed properly. The situation became better in the RV bottom temperature case. The variance of the calculation results reduced from the reduced, however, it did not show satisfying accordance. The discordance increased in the average RV temperature case, therefore, it could be inferred that proper ($T_{RV,representative} + \Delta T_{by\ boundary}$) exists between the average and minimum temperature of the RV. Therefore, the proper interpolation between the maximum and minimum temperature as ($0.2T_{RV,top} + 0.8T_{RV,bottom}$) was determined for ($T_{RV,representative} + \Delta T_{by\ boundary}$). The blending of the RV top and bottom temperature was suggested based on the cooling fraction of the near components. The RV top temperature was related to the cooling by the narrow gap, and the RV bottom temperature was related to the cooling by the lower plenum. Their cooling fraction was approximately 20% and 80%, respectively. Therefore, the blending ratio was first tried as 0.2 and 0.8, and the results were satisfactory. Although it is not certain, relationship between the blending factor and cooling fraction could be suggested.

Table 6
Determination of the proper $T_{RV,representative} + \Delta T_{by\ boundary}$.

Case	$T_{RV,top}$	$T_{RV,bottom}$	T_{RVavg}	$0.2T_{RV,top} + 0.8T_{RV,bottom}$
$40\Delta T_{ref}$	26.2 °C	36.2 °C	31.2 °C	34.2 °C
$60\Delta T_{ref}$	22.2 °C	37.1 °C	29.6 °C	34.1 °C
$80\Delta T_{ref}$	18.5 °C	38.4 °C	28.4 °C	34.4 °C
$100\Delta T_{ref}$	14.8 °C	39.6 °C	27.2 °C	34.7 °C

4. Conclusions

The natural circulation of the reactor pool under RVACS operation were analyzed in the SINCRO-2D. It was a two-dimensional, 1 : 25 reduced facility with water simulant. In general, the thermal stratification and entrainment effect of the natural circulation flow on the temperature distribution were observed. Cooling fraction of the narrow gap and lower plenum was approximately 0.2 and 0.8 respectively, and natural circulation was the dominant heat transfer mechanism even in the narrow gap region.

The effects of the decay heat and cooling boundary temperature distribution were parametrically studied. If decay heat changed, the magnitude of the temperature was changed in the pool, while its tendency of the distribution was maintained. Corresponding cooling fraction and characteristics of the natural circulation did not change. Thus, the decay heat effect could be treated as a multiplication of the temperature difference between the pool and cooling boundary. Regard to the boundary temperature distribution, which was simplified as the temperature difference between the top and bottom of the RV, it did not have significant effect on the pool distribution neither. The effect of the cooling boundary temperature distribution could be treated as global temperature offset of the whole pool. The offset was evaluated as ($0.2T_{RV,top} + 0.8T_{RV,bottom}$) including the RV temperature. It was suggested that the blending factor of the temperature had relationship with the cooling fraction of the nearby region.

Declaration of competing interest

The authors declare that they have no known competing financial interests or personal relationships that could have appeared to influence the work reported in this paper.

Acknowledgment

This work was supported by the Basic Science Research Program (NRF- 2020M2A8A4022882, 2021M2D2A1A03048950) through the National Research Foundation of Korea (NRF) funded by the Korea government, the Ministry of Science and ICT (MSIT).

References

[1] The Fukishima Daiichi Accident, IAEA, Vienna, 2015.
[2] G.J.V. Tuyle, Simplified analysis of PRISM RVACS performance without liner spill-over, in: Proceedings of International Topical Meeting on Fast Reactor Safety, 1990. Snowbird, UT, USA.
[3] W.K. Lehto, R.M. Fryer, E.M. Dean, J.F. Koenig, L.K. Chang, D. Mohr, E.E. Feldman, Safety analysis for the loss of flow and loss of heat sink without scram tests in EBR II, Nucl. Eng. Des. 101 (1987) 35–44.
[4] E.E. Feldman, D. Mohr, L.K. Chang, H.P. Planchon, E.M. Dean, P.R. Betten, EBR II unprotected loss of heat sink predictions and preliminary test results, Nucl. Eng. Des. 101 (1987) 57–66.
[5] D. Tenchine, D. Pialla, T.H. Fanning, J.W. Thomas, P. Chellapandi, Y. Shvetsov, L. Maas, H.Y. Jeong, K. Mikityuk, A. Chenu, H. Mochizuki, S. Monti, International benchmark on the natural convection test in Peonix reactor, Nucl. Eng. Des. 258 (2013) 189–198.
[6] D. Pialla, D. Tenchine, S. Li, P. Gauthe, A. Vasile, R. Baviere, N. Tauveron, F. Perdu, L. Maas, F. Cocheme, K. Huber, X. Cheng, Overview of the system alone and system/CFD coupled calculations of the PHENIX natural circulation test within the THINS project, Nucl. Eng. Des. 290 (2015) 78–86.
[7] J. Yoon, J. Lee, H. Kim, Y.B. Lee, ad J. Eoh, Heat transfer characteristics of redan structure in large-scale test facility STELLA-2, Nucl. Eng. Technol. 53 (2021) 1109–1118.
[8] S. Grewal, E. Gluekler, Water simulation of sodium reactors, Chem. Eng. Commun. 17 (1982) 343–360.
[9] Y. Ieda, H. Kamide, H. Ohshima, S. Sugawara, H. Ninokata, Strategy of experimental studies in PNC on natural convection decay heat removal, in: Proceedings of International IAEA-IWGFR Specialists' Meeting on Passive and Active Safety Features of LMFRs, 1991. Oarai, Ibaraki, Japan.
[10] Y. Eguchi, H. Takeda, T. Koga, N. Tanaka, K. Yamamoto, Quantitative prediction of natural circulation in an LMFR with a similarity law and a water test, Nucl. Eng. Des. 178 (1997) 295–307.

[11] M.H. Lee, D.W. Jerng, I.C. Bang, Experimental validation of simulating natural circulation of liquid metal using water, Nucl. Eng. Technol. 52 (2020) 1963–1973.
[12] H. Hoffman, K. Hain, K. Marten, H. Ohira, K. Rust, D. Weinberg, The status of thermal-hydraulic studies on the decay heat removal by natural convection using RAMONA and NEPTUN models, in: Proceedings of the 4th International Topical Meeting on Nuclear Thermal Hydraulics, Operation and Safety, 1994. Taipei, Taiwan.
[13] D. Weinberg, K. Rust, H. Hoffman, Overview report of RANONA-NEPTUN program on passive decay heat removal, No. FZKA–5667. Forschungszentrum Karlsruhe GmbH Technik und Umwelt (Germany), Inst. fuer Angewandte Thermo-und Fluiddynamik, 1996.
[14] H. Takeda, T. Koga, O. Watanabe, Experimental and computational simulation for natural circulation in an LMFBR, Nucl. Eng. Des. 140 (1993) 331–340.
[15] J.E. Cha, S.H. Lee, S.O. Kim, Y.I. Kim, Development of a Water Scaled Model for the Thermal Hydraulic Study of 600 MWe-SFR, Proceedings of the Korean nuclear society meeting, Pyeongchang, Korea, 2010.
[16] A. Ono, A. Kurihara, M. Tanaka, H. Oshima, H. Kamide, Study on Reactor Vessel Coolability of Sodium Cooled Fast Reactor under Severe Accident Condition Water Experiments Using a Scale Model –, ICAPP 2017, 2017. Fukui and Kyoto, Japan.
[17] P. Planquart, K. van Tichelen, Experimental investigation of accidental scenarios using a scale water model of a HLM reactor, Nucl. Eng. Des. 346 (2019) 10–16.
[18] Y. Nishi, I. Kinoshita, Study on decay heat removal capability of reactor vessel auxiliary cooling system, in: Proceedings of International IAEA-IWGFR Specialists' Meeting on Passive and Active Safety Features of LMFRs, 1991. Oarai, Ibaraki, Japan.
[19] G. Wu, M. Jin, J. Chen, Y. Bai, Y. Wu, Assessment of RVACS performance for small size lead-cooled fast reactor, Ann. Nucl. Energy 77 (2015) 310–317.
[20] C. Choi, T. Jeong, S. An, Thermal-hydraulic analyses of passive reactor vault cooling system (RVCS) in PGSFR using MARS-LMR, Ann. Nucl. Energy 117 (2018) 333–342.
[21] S. Yeom, J. Han, S. Ryu, D. Kim, J. Eoh, S. Choi, Design and evaluation of reactor vault cooling system in PGSFR, Nucl. Eng. Des. 365 (2020), 110717.
[22] A. Kraus, R. Hu, CFD simulations of natural convection cooling after a loss-of-flow transient, in: Proceedings of NURETH-16, Chicago, IL, August 30-September 4, 2015.